Validation of diffuse correlation spectroscopy measurements of rodent cerebral blood flow with simultaneous arterial spin labeling MRI; towards MRI-optical continuous cerebral metabolic monitoring

S. A. Carp,* G. P. Dai, D. A. Boas, M. A. Franceschini, and Y. R. Kim

Athinoula A. Martinos Center for Biomedical Imaging, Massachusetts General Hospital, Harvard Medical School, Charlestown, MA, 02129, USA

**carp@nmr.mgh.harvard.edu*

Abstract: Cerebral blood flow (CBF) during stepped hypercapnia was measured simultaneously in the rat brain using near-infrared diffuse correlation spectroscopy (DCS) and arterial spin labeling MRI (ASL). DCS and ASL CBF values agree very well, with high correlation (R=0.86, $p< 10^{-9}$), even when physiological instability perturbed the vascular response. A partial volume effect was evident in the smaller magnitude of the optical CBF response compared to the MRI values (averaged over the cortical area), primarily due to the inclusion of white matter in the optically sampled volume. The 8.2 and 11.7 mm mid-separation channels of the multi-distance optical probe had the lowest partial volume impact, reflecting $\sim$75 % of the MR signal change. Using a multiplicative correction factor, the ASL CBF could be predicted with no more than 10% relative error, affording an opportunity for real-time relative cerebral metabolism monitoring in conjunction with MR measurement of cerebral blood volume using super paramagnetic contrast agents.

OCIS codes: (170.2655) Functional monitoring and imaging; (170.1470) Blood or tissue constituent monitoring; (170.0170) Medical optics and biotechnology; (170.3340) Laser Doppler velocimetry.

References and links

1. G. R. Gordon, H. B. Choi, R. L. Rungta, G. C. Ellis-Davies, and B. A. MacVicar, "Brain metabolism dictates the polarity of astrocyte control over arterioles," Nature **456**, 745–749 (2008).
2. N. J. Maandag, D. Coman, B. G. Sanganahalli, P. Herman, A. J. Smith, H. Blumenfeld, R. G. Shulman, and F. Hyder, "Energetics of neuronal signaling and fMRI activity," Proc. Natl. Acad. Sci. U.S.A. **104**, 20546–20551 (2007).
3. I. Maurer, S. Zierz, and H. J. Moller, "Evidence for a mitochondrial oxidative phosphorylation defect in brains from patients with schizophrenia," Schizophr. Res. **48**, 125–136 (2001).
4. I. Maurer, S. Zierz, and H. J. Moller, "A selective defect of cytochrome c oxidase is present in brain of Alzheimer disease patients," Neurobiol. Aging **21**, 455–462 (2000).

#129409 - $15.00 USD Received 2 Jun 2010; revised 24 Jul 2010; accepted 24 Jul 2010; published 10 Aug 2010

5. M. Wong-Riley, P. Antuono, K. C. Ho, R. Egan, R. Hevner, W. Liebl, Z. Huang, R. Rachel, and J. Jones, "Cytochrome oxidase in alzheimer's disease: biochemical, histochemical, and immunohistochemical analyses of the visual and other systems," Vision Res. **37**, 3593–3608 (1997).
6. M. F. Beal, "Does impairment of energy metabolism result in excitotoxic neuronal death in neurodegenerative illnesses?" Ann. Neurol. **31**, 119–130 (1992).
7. A. M. Rudolph and M. A. Heymann, "The circulation of the fetus in utero. methods for studying distribution of blood flow, cardiac output and organ blood flow," Circ. Res. **21**, 163–184 (1967).
8. G. De Visscher, M. Haseldonckx, W. Flameng, M. Borgers, R. S. Reneman, and K. van Rossem, "Development of a novel fluorescent microsphere technique to combine serial cerebral blood flow measurements with histology in the rat," J. Neurosci. Methods. **122**, 149–156 (2003).
9. K. M. Powers, C. Schimmel, R. W. Glenny, and C. M. Bernards, "Cerebral blood flow determinations using fluorescent microspheres: variations on the sedimentation method validated," J. Neurosci. Methods. **87**, 159–165 (1999).
10. A. Humeau, W. Steenbergen, H. Nilsson, and T. Stromberg, "Laser doppler perfusion monitoring and imaging: novel approaches," Med. Biol. Eng. Comput. **45**, 421–435 (2007).
11. V. Rajan, B. Varghese, T. G. van Leeuwen, and W. Steenbergen, "Review of methodological developments in laser doppler flowmetry," Lasers Med. Sci. **24**, 269–283 (2009).
12. V. L. Babikian, E. Feldmann, L. R. Wechsler, D. W. Newell, C. R. Gomez, U. Bogdahn, L. R. Caplan, M. P. Spencer, C. Tegeler, E. B. Ringelstein, and A. V. Alexandrov, "Transcranial doppler ultrasonography: year 2000 update," J. Neuroimaging **10**, 101–115 (2000).
13. J. A. Detre, J. S. Leigh, D. S. Williams, and A. P. Koretsky, "Perfusion imaging," Magn. Reson. Med. **23**, 37–45 (1992).
14. T. T. Liu and G. G. Brown, "Measurement of cerebral perfusion with arterial spin labeling: Part 1. methods," J. Int. Neuropsychol. Soc. **13**, 517–525 (2007).
15. D. A. Boas, L. E. Campbell, and A. G. Yodh, "Scattering and imaging with diffusing temporal field correlations," Phys. Rev. Lett. **75**, 1855–1858 (1995).
16. D. A. Boas and A. G. Yodh, "Spatially varying dynamical properties of turbid media probed with diffusing temporal light correlation," J. Opt. Soc. Am. A **14**, 192–215 (1997).
17. T. Durduran, R. Choe, W. B. Baker, and A. G. Yodh, "Diffuse optics for tissue monitoring and tomography," Rep. Prog. Phys. **73**, 076701 (2010).
18. J. Li, G. Dietsche, D. Iftime, S. E. Skipetrov, G. Maret, T. Elbert, B. Rockstroh, and T. Gisler, "Noninvasive detection of functional brain activity with near-infrared diffusing-wave spectroscopy," J. Biomed. Opt. **10**, 44002 (2005).
19. C. Cheung, J. P. Culver, K. Takahashi, J. H. Greenberg, and A. G. Yodh, "In vivo cerebrovascular measurement combining diffuse near-infrared absorption and correlation spectroscopies," Phys. Med. Biol. **46**, 2053–2065 (2001).
20. J. P. Culver, T. Durduran, T. Furuya, C. Cheung, J. H. Greenberg, and A. G. Yodh, "Diffuse optical tomography of cerebral blood flow, oxygenation, and metabolism in rat during focal ischemia," J. Cereb. Blood Flow Metab. **23**, 911–924 (2003).
21. C. Zhou, S. A. Eucker, T. Durduran, G. Yu, J. Ralston, S. H. Friess, R. N. Ichord, S. S. Margulies, and A. G. Yodh, "Diffuse optical monitoring of hemodynamic changes in piglet brain with closed head injury," J. Biomed. Opt. **14**, 034015 (2009).
22. M. N. Kim, T. Durduran, S. Frangos, B. L. Edlow, E. M. Buckley, H. E. Moss, C. Zhou, G. Yu, R. Choe, E. Maloney-Wilensky, R. L. Wolf, M. S. Grady, J. H. Greenberg, J. M. Levine, A. G. Yodh, J. A. Detre, and W. A. Kofke, "Noninvasive measurement of cerebral blood flow and blood oxygenation using near-infrared and diffuse correlation spectroscopies in critically brain-injured adults," Neurocrit. Care **12**, 173–180 (2010).
23. N. Roche-Labarbe, S. A. Carp, A. Surova, M. Patel, D. A. Boas, P. E. Grant, and M. A. Franceschini, "Noninvasive optical measures of CBV, St_{O2}, CBF index, and $rCMRO_2$ in human premature neonates' brains in the first six weeks of life," Hum. Brain Mapp. **31**, 341–352 (2010).
24. E. M. Buckley, N. M. Cook, T. Durduran, M. N. Kim, C. Zhou, R. Choe, G. Yu, S. Schultz, C. M. Sehgal, D. J. Licht, P. H. Arger, M. E. Putt, H. H. Hurt, and A. G. Yodh, "Cerebral hemodynamics in preterm infants during positional intervention measured with diffuse correlation spectroscopy and transcranial doppler ultrasound," Opt. Express **17**, 12571–12581 (2009).
25. T. Durduran, G. Yu, M. G. Burnett, J. A. Detre, J. H. Greenberg, J. Wang, C. Zhou, and A. G. Yodh, "Diffuse optical measurement of blood flow, blood oxygenation, and metabolism in a human brain during sensorimotor cortex activation," Opt. Lett. **29**, 1766–1768 (2004).
26. T. Durduran, C. Zhou, E. M. Buckley, M. N. Kim, G. Yu, R. Choe, J. W. Gaynor, T. L. Spray, S. M. Durning, S. E. Mason, L. M. Montenegro, S. C. Nicolson, R. A. Zimmerman, M. E. Putt, J. Wang, J. H. Greenberg, J. A. Detre, A. G. Yodh, and D. J. Licht, "Optical measurement of cerebral hemodynamics and oxygen metabolism in neonates with congenital heart defects," J. Biomed. Opt. **15**, 037004 (2010).
27. G. Yu, T. F. Floyd, T. Durduran, C. Zhou, J. Wang, J. A. Detre, and A. G. Yodh, "Validation of diffuse correlation spectroscopy for muscle blood flow with concurrent arterial spin labeled perfusion mri," Opt. Express **15**, 1064–

#129409 - $15.00 USD Received 2 Jun 2010; revised 24 Jul 2010; accepted 24 Jul 2010; published 10 Aug 2010

1075 (2007).
28. S. Fantini, M.-A. Franceschini, J. S. Maier, S. A. Walker, B. B. Barbieri, and E. Gratton, "Frequency-domain multichannel optical detector for noninvasive tissue spectroscopy and oximetry," Opt. Eng. **34**, 32–42 (1995).
29. M. A. Franceschini, S. Thaker, G. Themelis, K. K. Krishnamoorthy, H. Bortfeld, S. G. Diamond, D. A. Boas, K. Arvin, and P. E. Grant, "Assessment of infant brain development with frequency-domain near-infrared spectroscopy," Pediatr. Res. **61**, 546–551 (2007).
30. G. Paxinos and C. Watson, *The rat brain in stereotaxic coordinates* (Academic Press, San Diego, 1998).
31. G. Strangman, M. A. Franceschini, and D. A. Boas, "Factors affecting the accuracy of near-infrared spectroscopy concentration calculations for focal changes in oxygenation parameters," Neuroimage **18**, 865–879 (2003).
32. T. Reich and H. Rusinek, "Cerebral cortical and white matter reactivity to carbon dioxide," Stroke **20**, 453–457 (1989).
33. M. Sato, G. Pawlik, and W. D. Heiss, "Comparative studies of regional cns blood flow autoregulation and responses to co2 in the cat. effects of altering arterial blood pressure and paco2 on rcbf of cerebrum, cerebellum, and spinal cord," Stroke **15**, 91–97 (1984).
34. M. Reivich, "Arterial pco2 and cerebral hemodynamics," Am. J. Physiol. **206**, 25–35 (1964).
35. D. A. Boas, J. P. Culver, J. J. Stott, and A. K. Dunn, "Three dimensional monte carlo code for photon migration through complex heterogeneous media including the adult human head," Opt. Express **10**, 159–170 (2002).
36. D. Boas, "Diffuse photon probes of structural and dynamical properties of turbid media : theory and biomedical applications," Ph.D. thesis, Univ. of Pennsylvania (1996).
37. C. Zhou, "In vivo optical imaging and spectroscopy of cerebral hemodynamics," Ph.D. thesis, Univ. of Pennsylvania (2007).
38. J. P. Culver, T. Durduran, C. Cheung, D. Furuya, J. H. Greenberg, and A. G. Yodh, "Diffuse optical measurement of hemoglobin and cerebral blood flow in rat brain during hypercapnia, hypoxia and cardiac arrest," Adv. Exp. Med. Biol. **510**, 293–297 (2003).
39. J. Lu, G. Dai, Y. Egi, S. Huang, S. J. Kwon, E. H. Lo, and Y. R. Kim, "Characterization of cerebrovascular responses to hyperoxia and hypercapnia using mri in rat," Neuroimage **45**, 1126–1134 (2009).
40. M. Fabricius and M. Lauritzen, "Examination of the role of nitric oxide for the hypercapnic rise of cerebral blood flow in rats," Am. J. Physiol. **266**, 1457–2464 (1994).
41. M. Fabricius, I. Rubin, M. Bundgaard, and M. Lauritzen, "Nos activity in brain and endothelium: relation to hypercapnic rise of cerebral blood flow in rats," Am. J. Physiol. **271**, 2035–2044 (1996).
42. S. Wegener, W. C. Wu, J. E. Perthen, and E. C. Wong, "Quantification of rodent cerebral blood flow (CBF) in normal and high flow states using pulsed arterial spin labeling magnetic resonance imaging," J. Magn. Reson. Imaging **26**, 855–862 (2007).
43. J. Mayhew, D. Johnston, J. Martindale, M. Jones, J. Berwick, and Y. Zheng, "Increased oxygen consumption following activation of brain: theoretical footnotes using spectroscopic data from barrel cortex," Neuroimage **13**, 975–987 (2001).
44. R. L. Grubb, M. E. Raichle, J. O. Eichling, and M. M. Ter-Pogossian, "The effects of changes in $PaCO_2$ on cerebral blood volume, blood flow, and vascular mean transit time," Stroke **5**, 630–639 (1974).
45. R. B. Buxton, E. C. Wong, and L. R. Frank, "Dynamics of blood flow and oxygenation changes during brain activation: the balloon model," Magn. Reson. Med. **39**, 855–864 (1998).
46. Y. Kong, Y. Zheng, D. Johnston, J. Martindale, M. Jones, S. Billings, and J. Mayhew, "A model of the dynamic relationship between blood flow and volume changes during brain activation," J. Cereb. Blood Flow Metab. **24**, 1382–1392 (2004).

1. Introduction

The cerebral metabolic rate of oxygen consumption ($CMRO_2$) is a physiological parameter closely linked to neural activation [1, 2], as well as to various disease states [3–6]. A key element necessary for $CMRO_2$ monitoring is a measure of cerebral blood flow (CBF). While bolus injection methods, using tracers such as radioactive [7] and fluorescent [8, 9] microspheres have proven quantitative accuracy, they only measure CBF at a few discrete timepoints. In addition to these steady state CBF measurements, accurate assessment of dynamic CBF changes with good temporal resolution provides a way to further understand neurohemodynamic coupling and metabolic parameters. Currently, continuous CBF monitoring can be achieved using Laser Doppler flowmetry (LDF) [10, 11], Transcranial Doppler Ultrasound (TCD) [12] or MRI-based Arterial Spin Labeling (ASL) [13, 14]. However, TCD can only give blood flow in large vessels, while LDF is an invasive technique requiring opening of the scalp and skull for probe placement. On the other hand, ASL provides an effective method for mapping CBF; however, the

#129409 - $15.00 USD Received 2 Jun 2010; revised 24 Jul 2010; accepted 24 Jul 2010; published 10 Aug 2010

technique is lacking in temporal resolution and sensitivity.

Diffuse correlation spectroscopy (DCS) [15–17], also known as Diffusing Wave Spectroscopy (DWS) [18] is a novel method for non-invasive CBF measurement at depth with excellent temporal resolution and sensitivity, especially effective in rodents, piglets and neonates. DCS cerebral blood flow measurements have been validated against LDF [19, 20], fluorescent microspheres [21], Xenon-CT [22], TCD [23, 24] and MRI-ASL [25, 26]. Outside the brain, DCS has also been validated against MRI-ASL for calf-muscle blood flow [27]. These encouraging results suggest DCS could be used for continuous non-invasive CBF estimation, and may be integrated with functional MRI methods for brain measurements.

In this work, we validate DCS against ASL measurements of CBF in the rat-brain using a graded hypercapnic challenge. We show strong linear correlation between DCS and ASL measures of blood flow and demonstrate DCS can be used together with a partial volume correction factor to recover the ASL data. We discuss the sources of the partial volume effect and suggest ways to minimize its size. Thus, we provide further proof of the feasibility of using DCS in conjunction with functional MRI in the brain.

2. Materials and Methods

2.1. Animal Preparation and Measurement Protocol

We used a total of seven adult male Sprague Dawley rats (Charles River, MA, USA; weight between 250 and 350 grams). Both left and right femoral veins (for infusion of anesthetics and contrast agent administration, respectively) and right femoral artery (for blood pressure monitoring and blood gas analysis) were catheterized. Animals were initially anesthetized with 2.0% isoflurane in 100% O_2, then tracheotomized and mechanically ventilated with 1.5% isoflurane in 70% N_2O/30% O_2 for the duration of surgery. Body temperature was measured with a rectal probe. Before the optical/MRI experiment, the anesthetic regimen was switched from the halothane gas mixture used for surgery to continuous infusion of α-chloralose (30 mg/kg/h), preceded by a loading bolus ($\sim$20 mg/kg). Concurrently with α-chloralose administration, rats were paralyzed with an intravenous bolus of pancuronium (1 mg/kg), which was followed by continuous infusion ($\sim$ 1.25 mg/kg/h) of pancuronium. Body temperature, blood oxygen saturation level, heart rate and blood pressure were monitored and carefully maintained at normal levels throughout the experiment. A temperature-controlled water blanket was placed under the rat's torso to maintain body temperature at 37.0 °C. A sufficient time was allowed for the anesthetic transition before the optical/MRI measurements. Blood gases (pO_2 and pCO_2) as well as pH were verified to be within normal ranges before the animal was inserted in the scanner cavity. Blood gas monitoring did not continue during the scans due to concerns over the need to use a lengthy ($>$1.5m) arterial sampling line as well as a lack of manpower to take and process samples while operating the optical and MR equipment. An additional two rats were later used as a control set using the same animal preparation procedure up through and including placing the rat in the scanner bore. However, we did not run the scanner or the optical measurement, thus being able to access the rat inside the scanner cage and allowing for a short (0.3 m) arterial line. Average blood gas values from these animals were used to estimate CO_2 reactivity in the main group under the assumption of similar behavior between the two sets.

The animals were mechanically ventilated at all times. The hypercapnic challenge involved exposure to a premixed gas consisting of 2.5, 5 or 7.5% CO_2 and 92.5, 95, 97.5% air, respectively. Each trial involved a 5 minutes baseline (100% air), 15 minutes stepped hypercapnia (5 minutes each at 2.5, 5, and 7.5% CO_2, respectively), followed by a 5 minute return to baseline. Each trial was repeated twice for each animal. Optical and MR acquisitions were continuously performed during the entire length of both trials.

#129409 - $15.00 USD Received 2 Jun 2010; revised 24 Jul 2010; accepted 24 Jul 2010; published 10 Aug 2010

2.2. *Near Infrared Cerebral Blood Flow Measurement*

We constructed a diffuse correlation spectrometer (DCS) system similar to the one developed by the Yodh group at Univ. of Pennsylvania [25]. A solid-state long coherence length laser at 785 nm (CrystaLaser RCL-785-080-S) was coupled to a 62.5μm multi-mode gradient index fiber and delivered to the tissue. The diffusely reflected light was collected by four single-mode optical fibers and detected by four photon-counting avalanche photodiodes (PC-APD, Perkin Elmer SPCM-AQR-14-FC). The intensity auto correlation function of each channel was computed by a digital correlator (Correlator.com Flex32-8ch) over a delay time range of 200 ns - 0.5 s. A correlation curve was acquired approx. 1.5 times per second. To improve the accuracy of the blood flow estimation the optical properties of the tissue were measured at the same time using a frequency domain near infrared spectrometer (FD-NIRS) [28, 29] using one source and four detector fiber bundles co-located with the DCS fibers, as described in section §2.4. The multi-distance FD-NIRS measurement was used to quantify the scattering and absorption coefficients by fitting said measurements to the standard diffusion approximation model for light transport in a semi-infinite turbid medium. The instruments operated in a time-interleaved fashion, where in each 15 second time interval, DCS data was acquired for 9 seconds at 1.5 Hz, followed by FD-NIRS data acquired for 6 seconds at 12.5 Hz.

2.3. *Arterial Spin Labeling MRI*

MRI measurements were performed using a horizontal bore 9.4 T Bruker/Magnex system, equipped with a home-built rat head surface RF transmitter and receiver coil, approximately 30 mm in diameter. A surface coil was used for brain imaging and a neck coil for perfusion labeling. Coil-to-coil electromagnetic interaction was actively decoupled. Simultaneous BOLD and CBF measurements were made using the two-coil continuous arterial spin-labeling method with single-shot, GE (TR/TE=3700/13 ms) echo planar imaging (EPI) acquisition (three 1 mm slices with inter-slice separation of 1 mm, FOV=2.3x2.3 cm^2, 64x64 matrix). Paired images were acquired alternately with and without arterial spin labeling.

2.4. *Hybrid Instrumentation and Combined Optical-MRI Probe*

A combined optical probe/MR coil assembly was fabricated to fit in the animal holder tube of the Bruker MRI system (Fig. 1). A plastic stereotactic frame held the animal's head fixed during the experiment. Both optical systems delivered and collected light through co-located source and detector fibers at 5.3, 8.2, 11.7 and 15.5 mm source-detector separations. The optical probe made of thermoplastic material is rigidly attached with two screws to the MR coil, thus giving reliable positioning of the optical fibers in the MR field of view. The acquisition start time was recorded to the second for all three instruments (DCS, FD-NIRS, MRI) as well as the gas change timing. It is expected that an approximately 30 second delay occurs before the gas change reaches the animal due to the length of the breathing gas lines.

2.5. *Data Analysis*

Four animals were used in the data analysis. Data from the other three could not be used because of hardware problems that resulted in poor labeling coil performance and subsequent low quality ASL images.

2.5.1. DCS data processing

The diffusion correlation equation offers the theoretical framework for analyzing the DCS data. As detailed by Boas et al. [15, 16] and further validated by Cheung et al., Culver et al. and Durduran et al. [19, 20, 25], the normalized intensity temporal auto-correlation function, $g_2(\tau)$

#129409 - $15.00 USD Received 2 Jun 2010; revised 24 Jul 2010; accepted 24 Jul 2010; published 10 Aug 2010

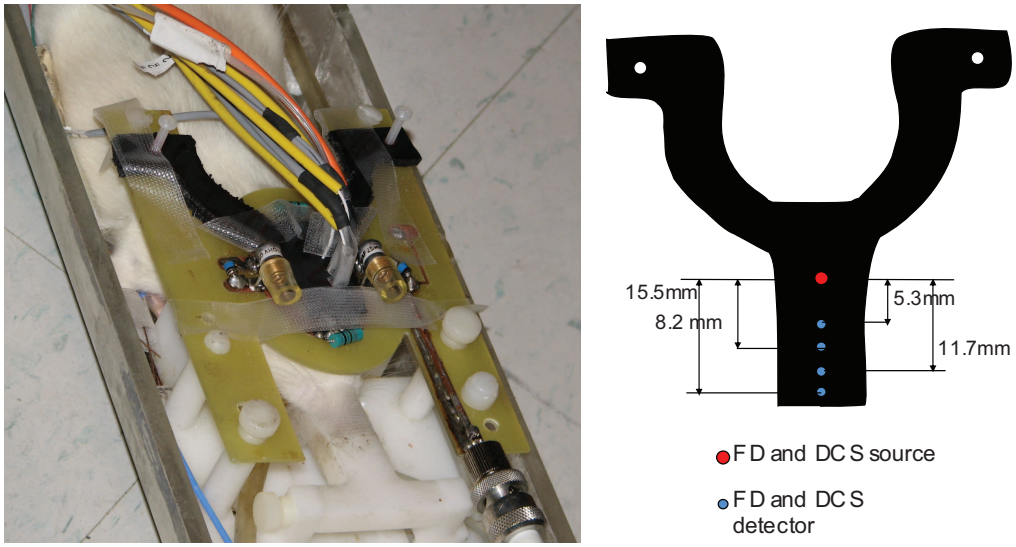

Fig. 1. Multi-modality probe design. a) Photograph of MRI head coil and optical probe assembly on a rat, ready to be inserted into the scanner bore; a separate ASL labeling coil is placed under the neck area. b) Schematic of optical probe, with fibers connected to both the FD-NIRS and the DCS system inserted at each location. Source position is shown in red, while detector positions are in blue, with source-detector separations of 5.3, 8.2, 11.7, and 15.5 mm, respectively

is given by:

$$g_2(r_s, r_d, \tau) = 1 + \beta \left[\exp\left(- \left(3\mu_s' \mu_a + P_{\mathrm{RBC}} \mu_s'^2 k_0^2 < \Delta r^2(\tau) > \right)^{1/2} \mid r_s - r_d \mid \right) \right]^2 \qquad (1)$$

where β is the coherence factor, r_s and r_d are the source and detector positions, respectively, τ is the correlation time, μ_s' is the reduced scattering coefficient, μ_a is the absorption coefficient, k_0 is the wavenumber for the laser light, P_{RBC} is the probability of scattering from a moving scatterer (most likely a red blood cell), and $< \Delta r^2(\tau) >$ is the mean square displacement of the moving scattering particles. Several studies [19, 25] have shown that DCS correlation profiles from living tissues can be fit well by assuming particle displacement follows Brownian motion dynamics:

$$< \Delta r^2(\tau) > = 6 D_b \tau \qquad (2)$$

where D_b is the Brownian diffusion coefficient. Since P_{RBC} is generally unknown, it is grouped together with D_b to form a blood flow index as $\mathrm{CBF}_{\mathrm{DCS}} = D_b P_{\mathrm{RBC}}$. To obtain the time-course of $\mathrm{CBF}_{\mathrm{DCS}}$ we first recover the absorption and scattering optical properties from the FD-NIRS instrument. These are then interpolated across the DCS timepoints and used in fitting Eqs. (1), (2) to the experimental measurements for each DCS source-detector pair individually.

#129409 - $15.00 USD Received 2 Jun 2010; revised 24 Jul 2010; accepted 24 Jul 2010; published 10 Aug 2010

2.5.2. MRI data processing

CBF maps have been created by subtracting tagged images from their untagged counterparts for each slice, resulting in a frame rate of one image every 7.4 seconds. Regions of interest were defined in the cortex in an area 2 mm wide under the location of the optical fibers. Because baseline blood flow was close to the system noise level, temporal traces were normalized to the average of the second half of the first 2.5% CO_2 period.

2.5.3. Comparison and correlation

The level of correlation of normalized time courses obtained from the two modalities was quantified using the Pearson product-moment correlation coefficient. Further, we calibrated the optical partial volume effect size over the entire measurement set, and estimated the accuracy in recovering ASL CBF measures from the DCS data.

3. Results

3.1. CBF response during stepped hypercapnia

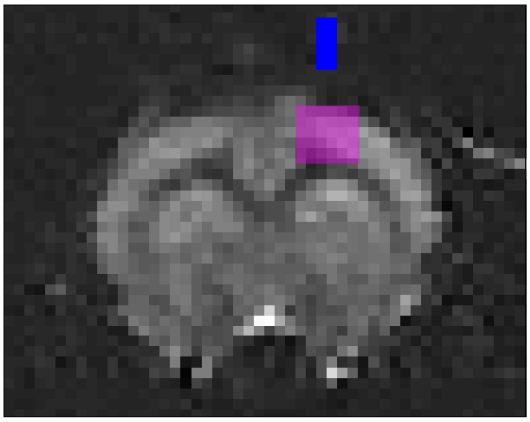

Fig. 2. ASL slice showing optical fiber locations (blue) and region-of-interest for averaging of MRI CBF (magenta)

Figure 2 shows a time-average of the middle ASL slice in one of the animals. The region of interest (ROI) used to obtain the MRI data is shown as a magenta rectangular overlay, while the location of the line of optical fibers is indicated using a blue filled rectangle above the MRI ROI. Figure 3 displays the average CO_2 response from N=4 stepped hypercapnia periods collected from multiple rats. Both MRI-ASL and DCS are included, and separate time-courses are plotted for each of the DCS channels (error bars represent standard errors). Values plotted are normalized to the average of the 2^{nd} half of the 2.5% CO_2 hypercapnia period, since the MRI-ASL data of that segment had the lowest standard deviation. A progressive increase in cerebral blood flow is noted for both measurement methods, as expected. The DCS CBF increase is lower compared to the ASL CBF, with the smallest increase displayed by the most superficially sensitive channel and very similar time-courses observed for the other three larger separation channels, with a small decrease at the largest separation. A summary of the observed relative CBF values is given in Table 1 (data averaged over the 2^{nd} half of each CO_2 level). The variations in optical absorption and scattering are much smaller than the increase in blood flow.

#129409 - $15.00 USD Received 2 Jun 2010; revised 24 Jul 2010; accepted 24 Jul 2010; published 10 Aug 2010

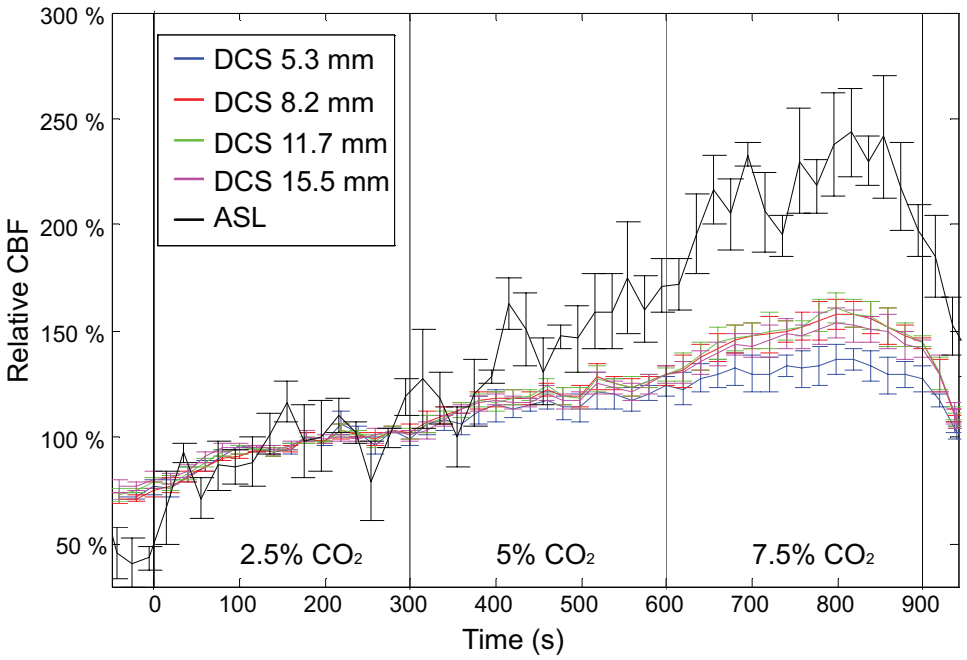

Fig. 3. Average normalized CBF time course for N=4 hypercapnia periods, from both ASL (black) and the 4 optical channels with 5.3 (blue), 8.2 (red), 11.7 (green) and 15.5 (magenta) mm separations, respectively; vertical bars indicate gas changes from 0→2.5 % CO_2, 2.5→5% CO_2, 5→7.5% CO_2 and 7.5→0% CO_2

The average changes with respect to the 0% CO_2 baseline at λ=785 nm are -0.76 ± 0.07%, 0.63 ± 0.64% and 2.41 ± 1.16%, respectively for μ_a, and 1.23 ± 0.07%, 2.41 ± 0.14% and 3.40 ± 0.16%, respectively for μ_s' at 2.5%, 5% and 7.5% inspired CO_2 volume fraction.

Table 1. Average relative CBF during stepped hypercapnia. Averages taken over the second half of each hypercania period. Baseline value for MRI-ASL is italicized to indicate lower confidence because of the lower SNR of the corresponding raw data.

	CO_2 level			
	0%	2.5%	5%	7.5%
DCS Ch.1 (5.3 mm)	72%	**100%**	118%	133%
DCS Ch.2 (8.2 mm)	71%	**100%**	124%	154%
DCS Ch.3 (11.7 mm)	75%	**100%**	124%	155%
DCS Ch.4 (15.5 mm)	78%	**100%**	122%	150%
MRI-ASL	*68%*	**100%**	150%	224%

While blood gases were not available for the animals reported in Table 1, the average pCO_2 values in the two animal control set were 38.2±4.2 mmHg, 43.2±4.7 mmHg, 54±6.3 mmHg, and 68.5±6.3 mmHg (mean ± stdev) for baseline, 2.5%, 5% and 7.5% CO2 respectively (average of 3 stepped hypercapnia trials on each rat). Making the assumption that these animals behaved similarly to the ones used as the main group, the CO_2 reactivity appears to be 3.74% / mmHg pCO_2 from the DCS data (average of ch.2 and 3) and 4.91% /mmHg pCO_2 for the ASL

#129409 - $15.00 USD Received 2 Jun 2010; revised 24 Jul 2010; accepted 24 Jul 2010; published 10 Aug 2010

data.

3.2. *Correlation of $rCBF_{DCS}$ and $rCBF_{ASL}$*

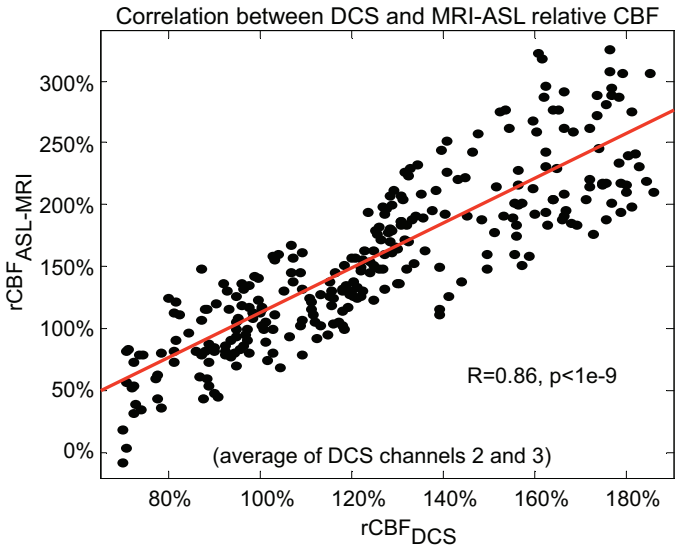

Fig. 4. DCS-ASL correlation scatter plot.

Figure 4 shows a scatter plot of relative CBF values measured with MRI-ASL and DCS during a representative stepped hypercapnia experiment, using the same normalization reference as the previous section. The DCS data represents an average of the two mid-separation DCS channels, which show the highest relative amount of response to hypercapnia. There is good linear agreement between the two methods, with a correlation coefficient R=0.86, and probability of no-correlation $p< 10^{-9}$. Table 2 summarizes the ratios between the fractional rCBF changes measured with DCS versus those measured with MRI-ASL. These ratios are calculated between 2.5% and 5% CO_2 and between 2.5% and 7.5% CO_2 levels, respectively and averaged over the same 4 stepped hypercapnia experiments used to generate Fig. 3. Note that, as shown in Table 2, DCS appears to always underestimate the ASL CBF change, more so at higher CBF values. The two mid-separation DCS channels (with inter-fiber distances of 8.2 and 11.7 mm respectively) reflect the ASL measurement best, with an average correction coefficient of 1.33 (i.e. $rCBF_{ASL}/\langle rCBF_{DCS}\rangle$=1.33). Finally, Table 3 gives the relative error encountered when using the the above correction coefficient to predict the ASL measured flow change from the mid-separation DCS data. Note that over the range of cerebral blood flows resulting from 2.5% to 7.5% hypercapnia, calibrated DCS measurements can predict MRI ASL rCBF values with no more than $\pm$10% relative error.

Table 2. Percent of MRI relative CBF change reflected by the DCS relative CBF change. Values less than 100% denote $rCBF_{DCS}$ underestimates $rCBF_{ASL}$

CO_2 level	DCS Ch.1	DCS Ch.2	DCS Ch.3	DCS Ch.4
5%	+79%	+83%	+83%	+81%
7.5%	+59%	+69%	+69%	+67%

#129409 - $15.00 USD Received 2 Jun 2010; revised 24 Jul 2010; accepted 24 Jul 2010; published 10 Aug 2010

Table 3. Error in predicting rCBF (normalized to CBF during the second half of the 2.5% CO_2 period)

	CO_2 level					
	2.5%		5%		7.5%	
	Prediction	Rel. Err.	Prediction	Rel. Err.	Prediction	Rel. Err.
DCS Ch.2	**100%**	N/A	165%	9.93%	205%	-8.58%
DCS Ch.3	**100%**	N/A	165%	9.93%	206%	-7.98%
MRI-ASL	**100%**	N/A	150%	N/A	224%	N/A

3.3. *Influence of physiological instability*

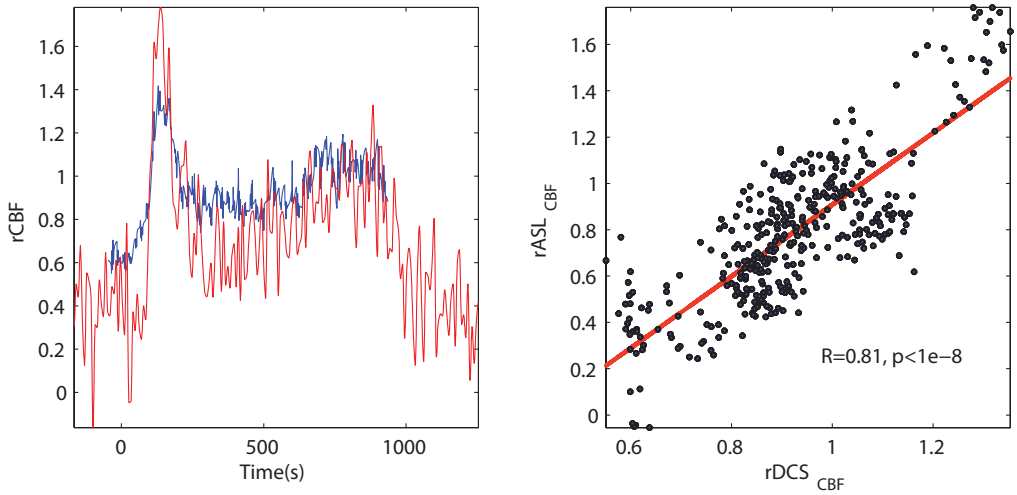

Fig. 5. CBF measurement during physiological instability. a) CBF time course from DCS (blue) and ASL (red) data; b) ASL vs DCS correlation plot

Figure 5 shows the relative CBF traces from ASL and the average of the mid-separation DCS channels (Ch. 2 and Ch. 3) during a stepped hypercapnia experiment affected by physiological instability. Specifically, the rat experienced a cortical spreading depression (CSD) wave evident in the full-frame time-resolved blood flow MR images (not shown). The temporal features of the two methods remain well aligned, while the scatter plot again indicates strong correlation, despite the CSD episode.

4. Discussion

Cerebral blood flow measurements are an essential component of cerebral oxygen metabolism monitoring. Diffuse correlation spectroscopy is the first optical method with the ability to quantify blood flow in thick tissue without the need for a contrast agent. Substantial effort has been expended to validate DCS [19–27] including previous validation against MRI ASL for calf muscle blood flow [27], cortical motor activation [25] and cerebral blood flow in neonates [26].

This study further validates DCS against ASL in the multi-layered environment of the intact rat brain. The DCS optical measure of blood flow, represented by the product $D_b P_{\mathrm{RBC}}$ exhibits good linear correlation with ASL data averaged over the field of view of the optical probe.

#129409 - $15.00 USD Received 2 Jun 2010; revised 24 Jul 2010; accepted 24 Jul 2010; published 10 Aug 2010

This correlation is maintained even in the presence of physiological instability, suggesting a link between the optical and MR flow measures at a fundamental level, as expected. While the linear relationship between $rCBF_{DCS}$ and $rCBF_{ASL}$ allows a simple multiplicative correction factor to be used to recover ASL variation values from DCS data, with good results as shown above, the significant underestimation of ASL CBF by DCS warrants further analysis.

There are two main possible sources of discrepancy – partial volume effects contaminating the cortical DCS signal and differences in the nature of the flow measurement between DCS and ASL. While analysis driven by segmented MRI structural images is beyond the scope of the current article, to further understand the magnitute of potential partial volume effects we might have encountered, we performed a set of Monte Carlo simulations on a flat layered geometry that mimicked the rat head. We used morphological data from the Paxinos and Watson rat brain atlas [30], the same probe fiber locations used for the hypercapnia experiments, a standard set of brain optical properties [31], and estimates of brownian diffusion coefficient for scalp and cortex from Li et al. [18]. Further we assumed that cortical blood flow doubles due to hypercapnic stimulation, while white matter has half of both the baseline perfusion and the CO_2 reactivity of the gray matter [32–34]. We employed the Monte Carlo code developed by Boas et al. [35] due to its ability to handle heterogeneous optical properties with a modification to additionally report momentum transfer accumulation along a photon path [36,37]. The simulated correlation decay profiles were then fitted using the same approach outlined in §2.5.1. From these simulations we found that all optical detectors collect photons that have sampled a significant amount of white matter with the proportion of white matter pathlength varying between 40% (Ch.1) to 70% (Ch.4). Further, scalp and skull account for 10-20% of the photon pathlenghts, leading to a 2% (Ch. 4) to 7% (Ch. 1) underestimation of cerebral blood flow. Finally, the only way to explain a significantly lower flow variation in the shortest source-detector separation as seen in our experimental data is to assume an air gap between the probe and the scalp of the rat. Such a 1-2 mm air gap likely occured due to the weight of the optical fibers bending the probe as the rat tube was inserted into the MR bore. Aside from the probable presence of the air gap, the main conclusions from the Monte Carlo simulations are that the most significant partial volume effect is due to the inclusion of a substantial amount of white matter in the photon migration path, while the skin and skull partial volume effect, even though present, has a minor impact. The influence of lower white matter baseline blood flow and CO_2 reactivity helps explain three important features of our results: a lower CBF increase seen by DCS compared to the cortically averaged MR ASL blood flow, a slightly reduced CBF response to CO_2 observed at the largest source-detector separation (Ch. 4) which is affected by the largest white matter partial volume effect, and the increasing discrepancy vs. ASL at 7.5% CO_2 compared to the 5% CO_2 level that likely results from the further increased perfusion contrast between the cortex and white matter at high inspired CO_2 concentration. The reduced CBF reponse at larger fiber separations has also been observed in the rat brain by Cheung et al. [19] for a 9 mm source-detector separation. Many of these caveats are related to the probe design and can be alleviated for future rat experiments by improving the rigidity of the probe and by reducing source detector separations. Note that we chose a fairly large probe fiber spacing to be able to maintain the accuracy of the diffusion approximation model used for FD-NIRS data analysis. However, Monte Carlo simulations and/or finite element methods could be used to relax this requirement and maintain accurate optical property recovery at short source detector distances.

Although the ability to explain many features of our results by using Monte Carlo simulations in a layered geometry is encouraging, these simulations predict at most a 15% reduction in measured DCS CBF vs. actual cortical blood flow for our probe fiber spacing in a typical rat, less than the 25% underestimation observed vs ASL-MRI. Further, the overall 0-7.5% CO_2 transition was accompanied by an average DCS CBF increase to 212% of the baseline, higher

#129409 - $15.00 USD Received 2 Jun 2010; revised 24 Jul 2010; accepted 24 Jul 2010; published 10 Aug 2010

than the 177% level reported by Cheung et al. [19] and Culver et al. [38] for a similar carbon dioxide level (8%), and the estimated 3.74% per mmHg pCO_2 reactivity is at the upper end of literature values which range between 2% and 4% per mmHg pCO_2 [39–41] (with the caveat that it was calculated using two different sets of animals). Finally, whereas Kim et al. [22] validated DCS CBF measurements against Xenon CT in an adult population noting only a 10% proportionality mismatch, Durduran et al. [26] presented DCS CBF validation data against MRI ASL in a neonatal population where the MRI ASL relative changes were 1.3 times bigger than the DCS relative CBF increase (as shown in Fig. 5 of the cited reference). Considering the totality of these observations – on one hand significant underestimation of ASL CBF measures by DCS, and the good agreement of DCS CBF with Xenon CT as well as literature CO_2 reactivity on the other hand – suggests there are perhaps structural differences in the way DCS and MRI-ASL measure tissue perfusion, related to their different mechanisms of sensitivity to flow. For example the ASL data may be affected by a perfusion related reduction in transit time, as well as hypercapnia induced blood oxygenation changes that modify local T_2* and thus image intensity [42]. Another potential source of error in the DCS CBF estimate relates to the way contributions from blood volume and blood flow velocity are reflected in the $P_{RBC}D_b$ quantity used as a blood flow index. CBF changes are the product of vessel cross-sectional area changes (linearly related to P_{RBC} under the assumption of constant length of the vessel network) and flow velocity changes (reflected by D_b). Since D_b is representative of root mean square displacement of scatterers in the blood, and not of their linear movement, it can be argued that the $P_{RBC}D_b$ product underestimates the impact of blood volume changes by a factor of $\sqrt{P_{RBC}}$, thus further explaining the underestimation of ASL CBF by the DCS method.

Combined DCS and FD-NIRS measurements can be used to estimate changes in cerebral metabolism using Fick's law, which is often expressed as $rCMRO_2$=rOEF.rCBF, where OEF is the oxygen extraction fraction, equal to the difference between the blood oxygen saturation on the arterial vs. venous side of a tissue region, and the prefix 'r' stands for relative change. The use of a compartmental model that assumes the measured tissue hemoglobin oxygen saturation is a mixture of arterial, capillary and venous blood [19, 43] in conjunction with DCS and NIRS data not corrected for partial volume effects has been met with success in several studies where $CMRO_2$ changes occur on a larger spatial scale, such as hypercapnia [19, 26], ischemia [20], or early brain development [23]. On the other hand, where metabolic changes are highly localized, such as during cerebral functional activation partial volume correction of the optical data appears necessary to obtain accurate $CMRO_2$ data [25].

The goal of the current publication is to suggest that DCS calibration against MRI-ASL can enable multi-modal MRI-optical continuous $CMRO_2$ monitoring during brain functional experiments, with potential improved relative metabolism quantification accuracy compared to current methods. The ability of the ASL technique to obtain fairly detailed perfusion images permits the calibration of the DCS flow measurement for a specific tissue volume that matches the area where functional activation occurs. Specifically, a stepped hypercapnia challenge can be performed at the beginning of the experimental protocol, leading to a set of correction coefficients that can convert DCS measurements into corresponding ASL blood flow changes for any particular cerebral region of interest. Then, the standard protocol for MR imaging of $CMRO_2$ can be followed, usually requiring the injection of a contrast agent for the determination of the cerebral blood volume. The DCS data can then be directly substituted for relative flow in the $rCMRO_2$ calculation, instead of using an assumed blood-volume blood-flow relationship such as the Grubb power law [44], which may result in significant errors in the assumed flow changes [45, 46]. A further advantage of using DCS for CBF quantification is the high temporal resolution of the optical methods, combined with good SNR for measurements at baseline flow rates. This is due to the fact that auto-correlation decay due to baseline flow is still much

#129409 - $15.00 USD Received 2 Jun 2010; revised 24 Jul 2010; accepted 24 Jul 2010; published 10 Aug 2010

faster than the decay due to any other source of biological or environmental fluctuation (DCS measurements taken post mortem show a correlation decay 3-4 orders of magnitude slower than before the animal is sacrificed).

5. Conclusion

We have demonstrated a strong linear relationship between diffuse correlation spectroscopy and MRI arterial spin labeling estimates of cerebral blood flow in the rat brain. While DCS measures underestimate the ASL changes, a multiplicative correction factor can be used to predict MRI flow changes from the DCS data. We propose that using stepped hypercapnia for DCS-ASL flow calibration can be used to enable multi-modal optical-MRI cerebral metabolism monitoring with improved accuracy vs. current methodology due to simultaneous blood flow and blood volume quantification as well as improved flow measurement noise, especially near baseline values.

Acknowledgements

Funding from National Institute of Health (NIH) grants R01EB006385, R01NS057476, R01EB001954, R01HD42908, P41RR014075, and R01EB002066.

#129409 - $15.00 USD Received 2 Jun 2010; revised 24 Jul 2010; accepted 24 Jul 2010; published 10 Aug 2010